

AAD-DCE: An Aggregated Multimodal Attention Mechanism for Early and Late Dynamic Contrast Enhanced Prostate MRI Synthesis.

Divya Bharti^{1*} Sriprabha Ramanarayanan^{1,2} Sadhana S¹ Kishore Kumar M¹ Keerthi Ram²
Harsh Agarwal³ Ramesh Venkatesan³ Mohanasankar Sivaprakasam^{1,2}

¹Indian Institute of Technology Madras (IITM), India
²Healthcare Technology Innovation Centre (HTIC), India
³GE HealthCare (GE), India

*b13.divya@gmail.com

Abstract—Dynamic Contrast-Enhanced Magnetic Resonance Imaging (DCE-MRI) is a medical imaging technique that plays a crucial role in the detailed visualization and identification of tissue perfusion in abnormal lesions and radiological suggestions for biopsy. However, DCE-MRI involves the administration of a Gadolinium-based (Gad) contrast agent, which is associated with a risk of toxicity in the body. Previous deep learning approaches that synthesize DCE-MR images employ unimodal non-contrast or low-dose contrast MRI images lacking focus on the local perfusion information within the anatomy of interest. We propose AAD-DCE, a generative adversarial network (GAN) with an aggregated attention discriminator module consisting of global and local discriminators. The discriminators provide a spatial embedded attention map to drive the generator to synthesize early and late response DCE-MRI images. Our method employs multimodal inputs - T2 weighted (T2W), Apparent Diffusion Coefficient (ADC), and T1 pre-contrast for image synthesis. Extensive comparative and ablation studies on the ProstateX dataset show that our model (i) is agnostic to various generator benchmarks and (ii) outperforms other DCE-MRI synthesis approaches with improvement margins of +0.64 dB PSNR, +0.0518 SSIM, -0.015 MAE for early response and +0.1 dB PSNR, +0.0424 SSIM, -0.021 MAE for late response, and (ii) emphasize the importance of attention ensembling. Our code is available at <https://github.com/bhartidivya/AAD-DCE>.

Index Terms—DCE-MRI, Aggregated Attention, Multimodal, Prostate Cancer

I. INTRODUCTION

Dynamic contrast-enhanced Magnetic Resonance Imaging (DCE-MRI) is a medical image scanning technique that quantifies tumor vasculature and perfusion characteristics [1]. The angiogenesis is captured by injecting a Gadolinium (Gad)-based contrast agent. This contrast agent exhibits a notable characteristic of rapid wash-in and wash-out kinetics occurring within a few seconds of Gad injection in the suspicious tissues, distinguishing it from normal healthy tissues. DCE-MRI plays a crucial role in prostate imaging, where the radiologists use a PI-RADS¹ score (in the scale 1 to 5) to assess the cancer

¹<https://www.acr.org/-/media/ACR/Files/RADS/PI-RADS/PIRADS-v2-1.pdf>

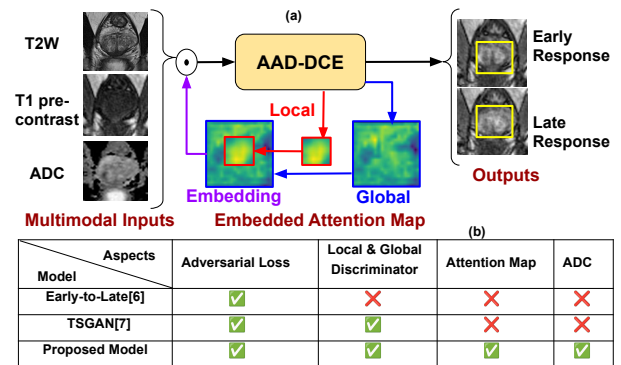


Fig. 1. (a) Concept diagram of AAD-DCE. Multimodal non-contrast inputs, with aggregated attention maps, synthesize early and late response DCE-MRI. (b) Previous DCE-MRI synthesis methods use adversarial training without focusing on key anatomical regions. The proposed approach integrates a discriminator-based global and local attention mechanism to enhance the generator’s performance.

severity by visualizing non-contrast images (T2 or diffusion-weighted images (DWI)). A score of 3 suggests DCE-MRI acquisition, which helps to reduce unnecessary biopsies by 25% [10], avoiding over-diagnosis of insignificant cancers. However, Gad-based contrast agents cause patient discomfort and other contraindications like Nephrogenic Systemic Fibrosis [2]. Therefore, there is a need to decrease the dosage or refrain from using a Gad-based contrast agent in DCE-MRI.

Deep learning methods have been explored for MRI reconstruction tasks ([20], [21]) and to reduce or eliminate the use of Gad-based DCE-MRI. The Generative Adversarial Network (GAN) [3] using a 3D U-Net-like generator produces 3D isotropic contrast-enhanced images from a 2D T2-flair image stack by adopting spatial pyramid pooling, enhanced residual blocks, and deep supervision. Retina U-Net [4] extracts the semantic features from non-contrast brain MR images and uses a synthesis module for contrast-enhanced images. The convolutional neural network (CNN) based network [5] generates full-dose late-response images from pre-contrast and low-

contrast images for brain MRI. A U-Net-based conditional-GAN [6] with residual loss function synthesizes late-response images from early-response breast MRI images. DCE-Diff [16] is a diffusion-based generative model that maps non-contrast to contrast-enhanced prostate images.

However, the former methods ([3], [4], [5], [6]) either depend on low-dose images or do not completely utilize the perfusion information from the non-contrast DCE-MRI data. In DCE-MRI, the Apparent Diffusion Coefficient (ADC) map computed using DWI carries useful information needed for generating the perfusion information. Secondly, the GAN-based methods adopt a global discriminator that is not specialized to consider the importance of local distribution related to the perfusion information within the anatomy of interest. DCE-Diff focuses on structural correlation without local context and suffers from higher computation costs for training and inference.

The goal of this work is to synthesize DCE-MRI early and late response images leveraging the complementary information from multimodal non-contrast MRI inputs and provide nuanced and detailed feature representation for perfusion (Fig. 1). Our method employs a GAN framework where the generator obtains additional guidance via an attention map computed and fed back from its discriminator. The attention map helps to focus more on the most discriminative areas between abnormal and healthy regions in the anatomy under study. Our method uses two discriminators to learn (i) the global structural correlation between the pre-contrast MRI and non-contrast T2 Weighted (T2W) MR images and (ii) local perfusion information using the ADC maps. In contrast, previous methods (TSGAN [7], ReconGLGAN [8]) use two discriminators for optimization without attention guidance.

We propose an Aggregated Attention-based discriminator (AAD) module consisting of two discriminators for global and local processing of the region of interest (ROI). The discriminators provide embedded spatial attention maps, each highlighting perfusion at fine and abstract levels. The two maps are aggregated and the ensembled map, rich in local details, guides the generator for improved synthesis of post-contrast images. Different from the previous attention-based discriminator [9], the proposed Aggregated Attention-based discriminator introduces a composition of attention maps to drive the generator. We summarize our contributions as follows: 1) An end-to-end trainable GAN for DCE-MR image synthesis from non-contrast multimodal MRI inputs, namely T2W, ADC, and T1 pre-contrast, with aggregated attention guidance to the generator to learn discriminative features that highlight hyperintense abnormal regions in the prostate anatomy. 2) A dual-discriminator framework with aggregated attention modules that (i) enables adversarial learning to capture both global and local perfusion characteristics of the prostate anatomy and (ii) learns an aggregated attention map that highlights essential details in the region of interest to guide the generator. Our discriminator is agnostic to varying generator architectures. 3) Extensive experiments on the ProstateX dataset demonstrate that the proposed model predicts early and late response

contrast-enhanced images with improvement margins (i)+0.64 dB PSNR, +0.0518 SSIM, -0.015 MAE for early response, and (ii) +0.1 dB PSNR, +0.0424 SSIM, -0.021 MAE for late response, surpassing the second best performing model, DCE-Diff. Our experiments highlight the importance of aggregated attention and ADC for accurate DCE-MRI synthesis.

II. PROPOSED METHOD

Our method is based on GAN, where a generator (G) and a discriminator (D) compete with each other to synthesize ground truth-like images from multi-modal input images. The core concept of AAD-DCE is to employ embedded spatial attention maps generated by the Aggregated Attention Discriminator (AAD) to guide the generator. This approach drives the generator to focus more on ROI, thus enhancing the post-contrast images. The input \mathbf{x} consists of T2W, ADC, and T1 pre-contrast images concatenated along the channel axis while \mathbf{y} represents the early and late response DCE-MR images as seen in Fig. 2(a).

A. Generator

The Generator (G) can be any image-to-image mapping CNN or transformer-based network. Our discriminator is adaptable to various generator architectures (Section III B). The generator architecture in Fig. 2(a), is an encoder-decoder architecture with residual blocks.

B. Aggregated Attention Discriminator (AAD)

The architecture of the AAD block is shown in Fig. 2(b). It consists of a Global Attention discriminator D_{GA} , a Local Attention discriminator D_{LA} , and a Classifier (Ψ_C). D_{GA} and D_{LA} are global and local feature extractors that employ a spatial guidance module named Attention Discriminator (AD). The input to D_{GA} is the whole image ($H \times W$) whereas D_{LA} operates only the ROI ($H' \times W'$). The AD in Fig. 2(c) comprises two key components: the Attention branch and the Trunk branch inspired by RAM [19]. The Trunk branch made up of convolutional layers, extracts low-level features from the input \mathbf{y} to produce the output $T(\mathbf{y})$. Note that our trunk branch is much simpler than in RAM [19] while maintaining feature extraction capability. The Attention branch, using the bottom-up top-down structure [18], learns an attention map $A(\mathbf{y})$, which modulates the trunk branch's output by applying weights. The output of D_{GA} and D_{LA} that utilizes the AD module are shown in (1) and (2),

$$E_G = (A_G(\mathbf{y}) + 1) \times T_G(\mathbf{y}) \quad (1)$$

$$E_L = (A_L(\mathbf{y}) + 1) \times T_L(\mathbf{y}) \quad (2)$$

where $A_G(\mathbf{y})$, $A_L(\mathbf{y})$ are the attention maps from attention branch and $T_G(\mathbf{y})$, $T_L(\mathbf{y})$ are trunk branch outputs for D_{GA} and D_{LA} respectively. The N_C dimensional feature vectors E_G and E_L are concatenated into a $2N_C$ dimensional vector and passed to the classifier (Ψ_C) as shown in (3). This vector is then fed into a fully connected layer, followed by a sigmoid activation function to classify real or fake.

$$D(\mathbf{y}) = \Psi_C(E_G || E_L) \quad (3)$$

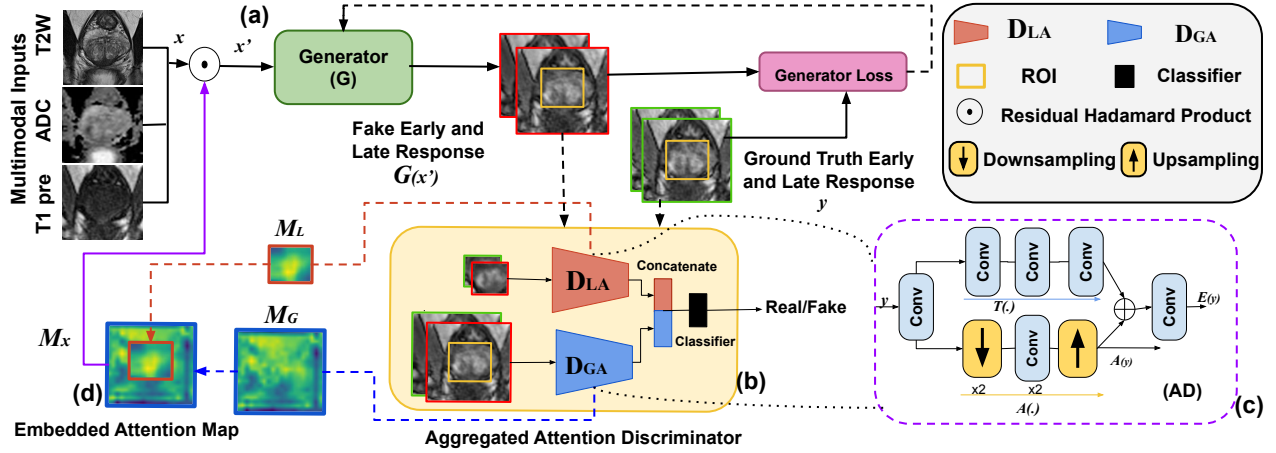


Fig. 2. (a) AAD-DCE architecture with a generator and an Aggregated Attention Discriminator (AAD) module. (b) AAD with local and global attention discriminators, D_{LA} and D_{GA} , respectively, utilizes (c) Attention Discriminator (AD) architecture. (d) Embedded attention map M_x .

TABLE I
QUANTITATIVE COMPARISON OF THE GENERATED EARLY AND LATE RESPONSE DCE-MRI IMAGES BETWEEN AAD-DCE AND OTHER MODELS.

Model	Early Response				Late Response			
	PSNR \uparrow	SSIM \uparrow	MAE \downarrow	FID \downarrow	PSNR \uparrow	SSIM \uparrow	MAE \downarrow	FID \downarrow
ConvLSTM	14.92 \pm 1.50	0.2397 \pm 0.04	0.139	118.706	15.27 \pm 2.56	0.2392 \pm 0.06	0.135	115.480
CycleGAN	18.61 \pm 1.90	0.5134 \pm 0.06	0.128	40.4371	17.20 \pm 2.40	0.4982 \pm 0.06	0.129	41.6501
Pix2Pix	19.53 \pm 1.97	0.5719 \pm 0.05	0.066	25.9182	19.35 \pm 1.94	0.5546 \pm 0.06	0.128	27.0816
RegGAN	20.56 \pm 0.02	0.5966 \pm 0.02	0.057	23.7963	19.89 \pm 0.02	0.5803 \pm 0.02	0.069	22.6124
TSGAN	21.16 \pm 3.50	0.6253 \pm 0.10	0.069	23.7533	20.08 \pm 2.64	0.5926 \pm 0.09	0.074	24.6665
ResViT	20.12 \pm 1.61	0.6308 \pm 0.05	0.063	32.4624	19.60 \pm 1.69	0.6153 \pm 0.05	0.070	30.0611
DCE-Diff	22.10 \pm 1.79	0.6700 \pm 0.05	0.040	10.5900	21.73 \pm 1.95	0.6500 \pm 0.06	0.050	7.2600
AAD-DCE	22.74 \pm 1.94	0.7218 \pm 0.05	0.025	18.5352	21.83 \pm 2.15	0.6924 \pm 0.06	0.029	19.8306

The mean value of the attention maps M_G and M_L obtained from the two discriminators, D_{GA} and D_{LA} are aggregated by embedding M_L into M_G to give M_x . M_x is infused into the multimodal inputs (x) using Residual Hadamard Product (RHP) as seen in (4) and fed to the Generator.

$$x' = (M_x + 1) \times x \quad (4)$$

As the infusion of attention map is based on RHP, it is initialized to one at the start of the training. The adversarial GAN loss, generator loss, and the final objective function are:

$$L_{GAN}(G, D) = \mathbb{E}_{y \sim \mathcal{Y}} [\log D(y)] + \mathbb{E}_{x \sim \mathcal{X}} [\log (1 - D(G(x')))] \quad (5)$$

$$L_{L1}(G) = \mathbb{E}_{x, y} [\|y - G(x')\|_1] \quad (6)$$

$$\arg \min_G \max_D L_{GAN}(G, D) + \lambda L_{L1}(G) \quad (7)$$

III. EXPERIMENTS AND RESULTS

A. Dataset and Implementation Details

We trained our model on the open-source ProstateX dataset [17] consisting of T2-Weighted, ADC, T1 pre-contrast, and DCE images. The dataset consists of 346 patient studies with 5520 images (4410 for training and 1104 for validation). In the DCE data, the early enhancement usually occurs within

10 seconds of the appearance of the injected contrast agent, and therefore, the early and late response time points are selected accordingly. The data is registered using SimpleITK rigid registration and is resampled to $H \times W \times 16$. Here $H \times W$ is 160×160 and $H' \times W'$ is 60×60 . We set N_C as 64.

TABLE II
IMPORTANCE OF ADC

DCE-MRI	Early Response		Late Response	
ADC	w/o ADC	w/ ADC	w/o ADC	w/ ADC
PSNR	21.50	22.74	20.43	20.64
SSIM	0.6841	0.7218	0.6404	0.6924

The models are trained using Pytorch 2.0 on a 24GB RTX 3090 GPU. The Adam optimizer ($\beta_1 = 0.9$, $\beta_2 = 0.999$, learning rate 1e-3) is used for 200 epochs, batch size of 4, and λ is 10. The evaluation metrics are Peak Signal-to-Noise Ratio (PSNR), Structural Similarity Index (SSIM), Mean Absolute Error (MAE), and Frechet Inception Distance (FID).

B. Results and Discussion

1. Comparative study with previous methods: We compare AAD-DCE with baseline models, Pix2Pix [11], CycleGAN [12], ConvLSTM [13], Reg-GAN [14], ResViT [15], TSGAN [7], and DCE-Diff [16]. The quantitative results in

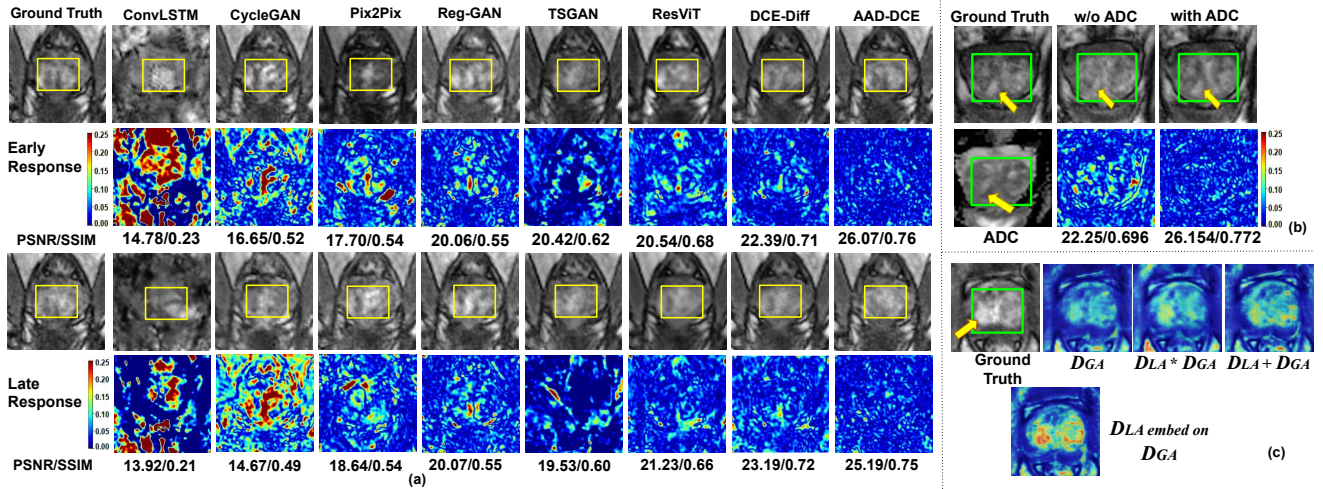


Fig. 3. (a) Visual results of early and late response for the ProstateX dataset with error maps. The yellow bounding box marks the ROI. (b) Ablative study with and without ADC maps. (c) Attention maps from different ensembling methods. Attention embedding enables better focus on suspicious regions.

TABLE III
ABLATIVE STUDY ON ATTENTION ENSEMBLING

Attention Maps	D_{GA}	$D_{LA} * D_{GA}$	$D_{LA} + D_{GA}$	D_{LA} embed on D_{GA}
PSNR	22.06	21.66	22.38	22.73
SSIM	0.7012	0.7014	0.7038	0.7218

Table I show that our model outperforms other GAN-based, transformer-based, and convLSTM methods in most cases. Our model outperforms DCE-Diff, by +0.64dB, +0.1 dB in PSNR, +0.0518, +0.0424 in SSIM, and -0.015, -0.021 in MAE for early and late response respectively, except in terms of FID due to diffusion models’ ability to learn image distribution through probabilistic framework. Fig. 3(a) illustrates the synthesis results highlighting the abnormal regions in the transition and peripheral zones (TZ and PZ) of the prostate. We observe that AAD-DCE is most comparable to the ground truth with fewer errors in the error map and better preserves the global and local details of the post-contrast images. We believe that: (i) While D_{GA} focuses on the overall anatomical features, D_{LA} targets the suspicious regions within the prostate via the attention information. (ii) ADC provides perfusion information, while T2W and T1 pre-contrast MR images establish the structural correlations. Integrating these modalities enables learning the complementary information, resulting in more accurate and detailed structural representations and perfusion information in the predicted images.

2. Importance of ADC: Table II shows the importance of using ADC as inputs. The incorporation of ADC images containing perfusion information improves the post-contrast image synthesis. Fig. 3(b) shows the abnormality in PZ that correlates with the tumor region findings in the ground truth (highlighted in yellow arrows).

3. Ablative study on attention ensembling: We study the effect of only the global attention and different ways of en-

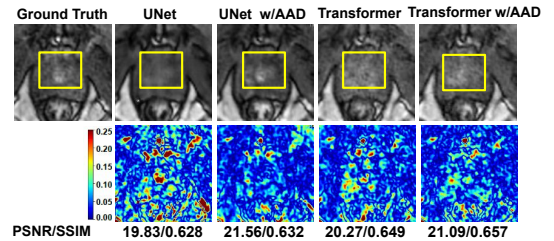


Fig. 4. Generator architecture with AAD enhances focus on the ROI.

sembling the global and local attention maps, namely additive, multiplicative, and embedding operations (Table III). In Fig. 3(c), the embedded attention map focuses more precisely on the regions with contrast uptake with greater clarity.

4. Ablative study on various generator architectures: We have evaluated the proposed AAD on various generator benchmarks - encoder-decoder CNN (U-Net) [11], vision transformer [15]. A U-Net with AAD improves PSNR by +1.49 dB and SSIM by +0.0387, while for the transformer-based generator, AAD provides improvements of +1.77 dB in PSNR and +0.0432 in SSIM (Fig. 4).

5. Model Parameters: Comparing with the recent state-of-the-art, DCE-Diff, shows that our model has 19.93 million parameters with superior performance over DCE-Diff with 125.08 million parameters.

IV. CONCLUSION

This work presents a GAN framework with aggregated attention feedback guidance to the generator from the discriminator to synthesize DCE-MR images from multimodal non-contrast MRI inputs. Extensive experimentation with comparative models and ablation studies with ADC, attention ensembling methods, and various generator architectures show that the proposed method can synthesize higher-quality DCE-MR images. We are currently aiming at clinical validation studies for practical use.

REFERENCES

- [1] Mazaheri, Yousef, Oguz Akin, and Hedvig Hricak. "Dynamic Contrast-enhanced Magnetic Resonance Imaging of Prostate Cancer: A Review of Current Methods and Applications." *World Journal of Radiology* 9, no. 12, pp. 416-425, 2017.
- [2] Moshe Rogosnitzky and Stacy Branch, "Gadolinium-based contrast agent toxicity: a review of known and proposed mechanisms," *Biometals*, vol. 29, no. 3, pp.365–376, 2016.
- [3] Wang, Y., Wu, W., Yang, Y., Hu, H., Yu, S., Dong, X., Chen, F., & Liu, Q, "Deep learning-based 3D MRI contrast-enhanced synthesis from a 2D non-contrast T2Flair sequence", *Medical Physics*, 49(7), pp. 4478–4493, 2022.
- [4] Xie, H., Lei, Y., Wang, T., Roper, J., Axente, M., Bradley, J. D., Liu, T., & Yang, X, "Magnetic resonance imaging contrast enhancement synthesis using cascade networks with local supervision", *Medical Physics*, 49(5), pp. 3278–3287, 2022.
- [5] Enhao Gong, M. John, Max Wintermark Pauly, and Greg Zaharchuk, "Deep learning enables reduced gadolinium dose for contrast-enhanced brain MRI," in *Journal of Magnetic Resonance Imaging*, vol. 48, pp. 330–340, 2018
- [6] J. C. Caicedo R. D. Fonnegra, M. Liliana Hernandez and G. M. Díaz, "Early-to-late prediction of DCE-MRI contrast-enhanced images in using generative adversarial networks," in *2023 IEEE 20th International Symposium on Biomedical Imaging*, pp. 1–5, 2023.
- [7] E. Kim, H. -H. Cho, J. Kwon, Y. -T. Oh, E. S. Ko and H. Park, "Tumor-Attentive Segmentation-Guided GAN for Synthesizing Breast Contrast-Enhanced MRI Without Contrast Agents," in *IEEE Journal of Translational Engineering in Health and Medicine*, vol. 11, pp. 32-43, 2023
- [8] Murugesan, B., S, V.R., Sarveswaran, K., Ram, K., Sivaprakasam, M, "Recon-GLGAN: A Global-Local context based Generative Adversarial Network for MRI Reconstruction," *Machine Learning for Medical Image Reconstruction Workshop, MLMIR 2019*, held in conjunction with MICCAI, pp. 3-15, 2019.
- [9] Lin, Y., Wang, Y., Li, Y., Gao, Y., Wang, Z. and Khan, L., 2021. Attention-based spatial guidance for image-to-image translation. In *Proceedings of the IEEE/CVF Winter Conference on Applications of Computer Vision*, pp. 816-825, 2021.
- [10] S. G. Armato et al., "PROSTATEx Challenges for computerized classification of prostate lesions from multiparametric magnetic resonance images," *Journal of Medical Imaging*, vol. 5, no. 04, p. 1, Nov. 2018, doi: 10.1117/1.jmi.5.4.044501.
- [11] P. Isola, J.-Y. Zhu, T. Zhou, and A. A. Efros, "Image-to-Image translation with conditional adversarial networks," In *Proceedings of the IEEE Conference on Computer Vision and Pattern Recognition*, pp. 1125-1134, 2017.
- [12] J.-Y. Zhu, T. Park, P. Isola, and A. A. Efros, "Unpaired Image-to-Image Translation Using Cycle-Consistent Adversarial Networks", *IEEE/ICCV*, pp.2223-2232, 2017.
- [13] Xingjian GulrajSHI, Zhouong Chen, Hao Wang, DitYan Yeung, Wai-kin Wong, and Wang-chun WOO, "Convolutional lstm network: A machine learning approach for precipitation nowcasting," in *Advances in Neural Information Processing Systems*, vol. 28, 2015.
- [14] L. Kong, C. Lian, D. Huang, Y. Hu, and Q. Zhou, "Breaking the dilemma of medical image-to-image translation," in *Advances in Neural Information Processing Systems*, vol. 34, pp. 1964–1978, 2021.
- [15] O. Dalmaz, M. Yurt, and T. Cukur, "RESVIT: Residual Vision Transformers for multimodal medical Image synthesis," *IEEE Transactions on Medical Imaging*, vol. 41, no. 10, pp. 2598–2614, Oct. 2022.
- [16] S. Ramanarayanan, A. Sarkar, MN. Gayathri, K. RAM, M. Sivaprakasam, "DCE-Diff: Diffusion Model for Synthesis of Early and Late Dynamic Contrast-Enhanced MR Images from Non-Contrast Multimodal Inputs," In *Proceedings of the IEEE/CVF Conference on Computer Vision and Pattern Recognition*, pp. 5174-5183, 2024.
- [17] Oscar Debats Geert Litjens, Nico Karssemeijer Jelle Barentsz, and Henkjan Huisman, "Prostatex Challenge data," in *The Cancer Imaging Archive*, 2017.
- [18] A. Newell, K. Yang, and J. Deng. Stacked hourglass networks for human pose estimation. *arXiv preprint arXiv:1603.06937*, 2016.
- [19] Fei Wang, Mengqing Jiang, Chen Qian, Shuo Yang, Cheng Li, Honggang Zhang, Xiaogang Wang, and Xiaoou Tang. "Residual attention network for image classification", In *CVPR*, pp. 3156–3164, 2017.
- [20] S. Ramanarayanan, B. Murugesan, K. Ram, and M. Sivaprakasam, "DC-WCNN: A deep cascade of Wavelet based convolutional neural networks for MR image Reconstruction," *IEEE 19th International Symposium on Biomedical Imaging (ISBI)*, pp. 1069-1073, 2022.
- [21] Y. Beauferris et al., "Multi-Coil MRI Reconstruction Challenge—Assessing brain MRI reconstruction models and their generalizability to varying coil configurations," *Frontiers in Neuroscience*, vol. 16, Jul. 2022.